Hyperpolarization without persistent radicals for in vivo real-time metabolic imaging

Tim R. Eichhorn[a,b,1], Yuhei Takado[a,1], Najat Salameh[a], Andrea Capozzi[a], Tian Cheng[a], Jean-Noël Hyacinthe[c], Mor Mishkovsky[d,e], Christophe Roussel[f], and Arnaud Comment[a,2]

[a]Institute of Physics of Biological Systems, Ecole Polytechnique Fédérale de Lausanne, CH-1015 Lausanne, Switzerland; [b]Paul Scherrer Institut, CH-5232 Villigen PSI, Switzerland; [c]Department of Radiology, Geneva University Hospital and Faculty of Medicine, University of Geneva, CH-1211 Genève 4, Switzerland; [d]Laboratory for Functional and Metabolic Imaging, Ecole Polytechnique Fédérale de Lausanne, CH-1015 Lausanne, Switzerland; [e]Department of Radiology, University of Lausanne, CH-1015 Lausanne, Switzerland; and [f]Section of Chemistry and Chemical Engineering and Institute of Chemical Sciences and Engineering, Ecole Polytechnique Fédérale de Lausanne, CH-1015 Lausanne, Switzerland

Edited* by Charles P. Slichter, Center for Advanced Study, University of Illinois Urbana–Champaign, Urbana, IL, and approved September 27, 2013 (received for review August 7, 2013)

Hyperpolarized substrates prepared via dissolution dynamic nuclear polarization have been proposed as magnetic resonance imaging (MRI) agents for cancer or cardiac failure diagnosis and therapy monitoring through the detection of metabolic impairments in vivo. The use of potentially toxic persistent radicals to hyperpolarize substrates was hitherto required. We demonstrate that by shining UV light for an hour on a frozen pure endogenous substance, namely the glucose metabolic product pyruvic acid, it is possible to generate a concentration of photo-induced radicals that is large enough to highly enhance the ^{13}C polarization of the substance via dynamic nuclear polarization. These radicals recombine upon dissolution and a solution composed of purely endogenous products is obtained for performing in vivo metabolic hyperpolarized ^{13}C MRI with high spatial resolution. Our method opens the way to safe and straightforward preclinical and clinical applications of hyperpolarized MRI because the filtering procedure mandatory for clinical applications and the associated pharmacological tests necessary to prevent contamination are eliminated, concurrently allowing a decrease in the delay between preparation and injection of the imaging agents for improved in vivo sensitivity.

nuclear magnetic resonance | metabolism | pyruvate | lactate | acetate

Magnetic resonance (MR) is a very powerful imaging modality in terms of temporal and spatial resolution of anatomical structures. The modality is widespread, well established in clinical environments, and paramagnetic agents are used extensively for enhanced contrast or perfusion examination. MR is also a unique technique to obtain in vivo metabolic maps using the spectroscopic information that can be extracted from the time-domain acquisitions. In particular, it is possible to monitor the biochemical transformations of specific substrates that are delivered to subjects. Because it gives access to the kinetics of the conversion of substrates into metabolites, MR spectroscopy (MRS) of the carbon nuclei (^{13}C) is one of the most powerful techniques to investigate intermediary metabolism (1).

The well-known weakness of MR as a spectroscopic technique is its relatively low sensitivity. It can be offset by so-called hyperpolarization methods, in particular the one based on dynamic nuclear polarization (DNP) (2), which is now commonly referred to as dissolution DNP and was first proposed about a decade ago (3). The hyperpolarized substrates obtained following dissolution DNP are biomolecules in aqueous solution with a largely out-of-equilibrium nuclear spin polarization corresponding to an enhancement of several orders of magnitude compared with the thermal equilibrium polarization attainable in MRI scanners. A basic requirement for DNP is the presence of unpaired electron spins in the sample to be hyperpolarized. These polarizing agents are usually incorporated in the form of persistent radicals. An inherent limit of any hyperpolarization method is that the intrinsic longitudinal nuclear spin relaxation will annihilate the polarization enhancement in the course of time to reach thermodynamic equilibrium. Relaxation will be accelerated by the presence of paramagnetic impurities such as persistent radicals. Most hyperpolarized substrates studied so far using dissolution DNP have a useful time window of the order of a minute, but within that window the method provides an unprecedented time resolution for the detection of intermediate metabolites in vivo (4–8). For in vivo applications, the presence of persistent radicals in the final dissolved product is also unwanted for physiological reasons. A filtering procedure is thus mandatory for clinical applications and the associated pharmacological tests necessary to prevent contamination increase the delay between preparation and injection of the imaging agents leading to reduced in vivo sensitivity.

To date, most preclinical developments have focused on samples of neat pyruvic acid (PA) to which suitable persistent radicals are added (6, 9–16). In the dissolution step of the dissolution DNP method, the acid is transformed into its salt in physiological buffer. This molecule has a central position in the glycolytic pathway: it connects glucose to lactate, alanine, and acetyl coenzyme A. It has already been demonstrated in several animal models that hyperpolarized pyruvate is a powerful marker for cancer metabolism, in particular because the increased lactate levels consequence of the Warburg effect can be readily detected (17). The results of the first human study performed on prostate cancer patients were recently published and it was shown that most of the trityl radicals used to polarize PA can be filtered out before injection (18).

Significance

Hyperpolarization is a significant development in MRI because it allows for imaging different metabolites in real time in vivo. There are no fundamental obstacles to rapid translation of this technique. Yet, to date, it has been necessary to use persistent radicals that need to be filtered out before injection and require pharmacological tests, which slow down the overall protocol, leading to reduced sensitivity. The demonstration that it is possible to prepare purely endogenous MRI agents to probe metabolism in vivo without using any potentially toxic compounds is a substantial step forward toward clinical radiology free of side effects.

Author contributions: T.R.E., C.R., and A. Comment designed research; T.R.E., Y.T., N.S., A. Capozzi, T.C., J.-N.H., and M.M. performed research; T.R.E., Y.T., N.S., A. Capozzi, T.C., J.-N.H., and M.M. analyzed data; and A. Comment wrote the paper.

The authors declare no conflict of interest.

*This Direct Submission article had a prearranged editor.

[1]T.R.E. and Y.T. contributed equally to this work.

[2]To whom correspondence should be addressed. E-mail: arnaud.comment@epfl.ch.

This article contains supporting information online at www.pnas.org/lookup/suppl/doi:10.1073/pnas.1314928110/-/DCSupplemental.

www.pnas.org/cgi/doi/10.1073/pnas.1314928110

Results and Discussion

In this article, we describe a variant of dissolution DNP that is based on pure PA samples without explicit addition of persistent radicals. We show that by UV irradiation of frozen neat PA, radicals are created in a concentration suitable for DNP (Fig. 1*A*). Their most compelling feature in the framework of hyperpolarized MR is that they recombine to biocompatible nonradical species within a fraction of a second upon dissolution: the carboxylic group of PA is cleaved, leading to carbon dioxide and another molecule subsequently transformed in acetic acid.

In aqueous solution, PA undergoes efficient photodecarboxylation from an excited triplet state (19, 20). The radicals produced by the low-temperature UV irradiation of the pure acid herein proposed (*Methods*) are most likely related to intermediary products postulated for this photodecarboxylation mechanism. The electron spin resonance (ESR) spectrum observed in frozen natural abundance PA following UV irradiation (Fig. 1*B*) can be readily interpreted by taking into account three equivalent and isotropic hyperfine couplings to the protons of the PA methyl group. A further isotropic hyperfine coupling to ^{13}C is observed when [1-^{13}C]PA is used (Fig. 1*C*). The ESR signal thus originates from an electron located in the orbital of a PA molecule from which one electron has been extracted.

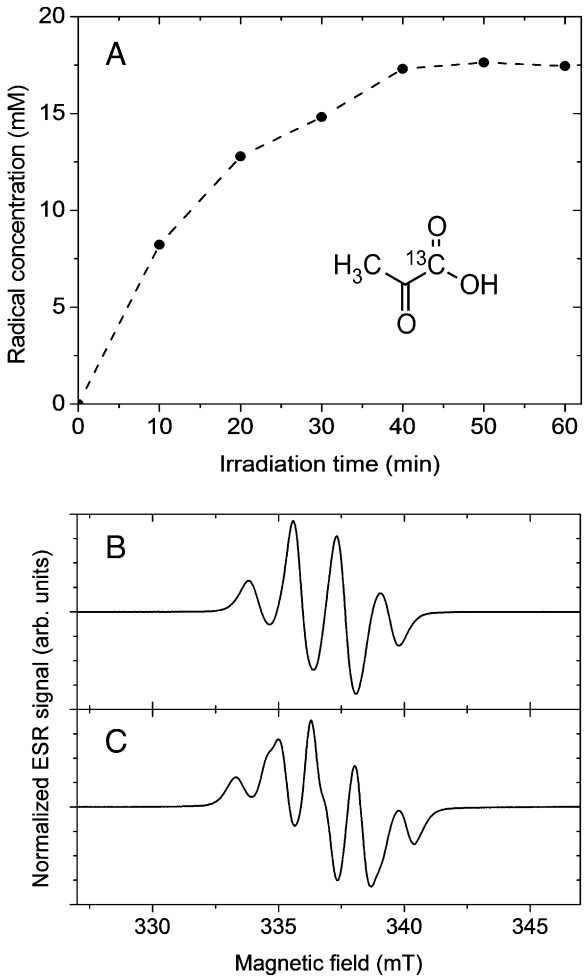

Fig. 1. Radical generation and ESR analysis at 77 K (*A*) Radical concentration in pure PA as a function of UV irradiation time as determined by X-band ESR. (*Inset*) Structural formula of [1-^{13}C]PA. (*B*) X-band ESR spectrum of natural abundance PA after 60 min of UV irradiation. (*C*) X-band ESR spectrum of [1-^{13}C]PA after 60 min of UV irradiation.

We have strong evidence from ^{13}C high-resolution room-temperature MR measurements performed on UV-irradiated frozen [U-^{13}C]PA dissolved in D_2O at 900 mM that the only products of recombination are $^{13}CO_2$ and [1,2-$^{13}C_2$]acetate (Fig. 2). Although it was suggested in a very early report that acetic acid could be a by-product of the photodecarboxylation of PA (21), it was never experimentally detected. Acetate is naturally present in human blood at a concentration of 0.05–0.2 mM in healthy subjects (22). The acetate concentration in the hyperpolarized pyruvate solution being about 600× lower than the one of pyruvate (*Methods*), an 80-mM pyruvate solution will only contain around 0.13 mM of acetate, meaning that its concentration will be kept at a normal physiological level following injection. In addition, with the most widely used substrate, namely [1-^{13}C]pyruvate, the resulting acetate molecule is unlabeled and its contribution to the ^{13}C signal will be completely negligible at such low concentrations. In fact, the label ends up in $^{13}CO_2$ gas, which is expelled from the solution during the extraction of the dissolved frozen sample from the hyperpolarizer with helium gas (dissolved $^{13}CO_2$ was observed in the spectrum shown in Fig. 2 because the frozen sample was simply melted in D_2O and not degassed or flushed with helium gas). As a consequence, not only is the solution free of paramagnetic impurities (no ESR signal was observable after dissolution and the in vitro ^{13}C T_1 was as long as in pure aqueous solution; Fig. S1), but all potential toxicity issues associated with the presence of radicals or by-products from the UV irradiation are also alleviated.

The width of the ESR spectrum (Fig. 1 *B* and *C*) suggests that the radical created by the proposed UV-irradiation procedure is of the "narrow-line" type according to the classification proposed in an earlier publication (23). The microwave spectrum measured by ^{13}C MR at 4.2 K extends over a frequency range about 2× wider than for samples prepared with the commonly used trityl radical, but is roughly 2× narrower than the microwave spectrum measured in samples prepared with a standard nitroxyl radical (Fig. 3). As expected, the performance of the radical created by UV irradiation for ^{13}C dissolution DNP is intermediate between that of trityl and nitroxyl radicals. A ^{13}C polarization of 10 ± 1% could be achieved in samples containing 17.5 ± 0.3 mM of radical within 2.5 h at 5 T and 1.2 ± 0.05 K using 50-mW microwave power. Under similar field and temperature conditions, it was shown that a ^{13}C polarization of up to 60% can be reached within the same amount of time using an optimal concentration of trityl radicals (24). Although the optimal concentration was not determined for the radicals created by UV irradiation, it is very likely that the ^{13}C polarization can be improved by increasing their concentration. This can for instance be done by diluting PA in water before UV irradiation and we observed that the radical concentration in a frozen 7.7-M aqueous PA solution is larger by more than 50% (Fig. S2). Deuteration of PA should also lead to larger ^{13}C polarization because the ESR line width of the photo-induced radicals is expected to be substantially narrower due to the lower hyperfine coupling to the deuterated methyl group.

To demonstrate the potential of the herein-presented method for generating imaging agents for in vivo MR, 80-mM hyperpolarized pyruvate solutions were prepared from UV-irradiated [1-^{13}C]PA samples using the hardware described in earlier publications (23, 25). A 300-μL bolus was injected into a mouse femoral vein (n = 3) before acquiring real-time metabolic ^{13}C spectra and images. A ^{13}C spectrum localized in the mouse head was measured every 3 s and, as previously reported, following the injection of pyruvate hyperpolarized with persistent radicals, [1-^{13}C]lactate, [1-^{13}C]alanine and $H^{13}CO_3^-$ signals were observed (Fig. 4*A*). The large signal-to-noise ratio (SNR) allowed us to perform real-time metabolic imaging with a 5-mm^3 spatial resolution and a 3-s time resolution by using a balanced steady-state free precession (bSSFP) sequence with selective excitations

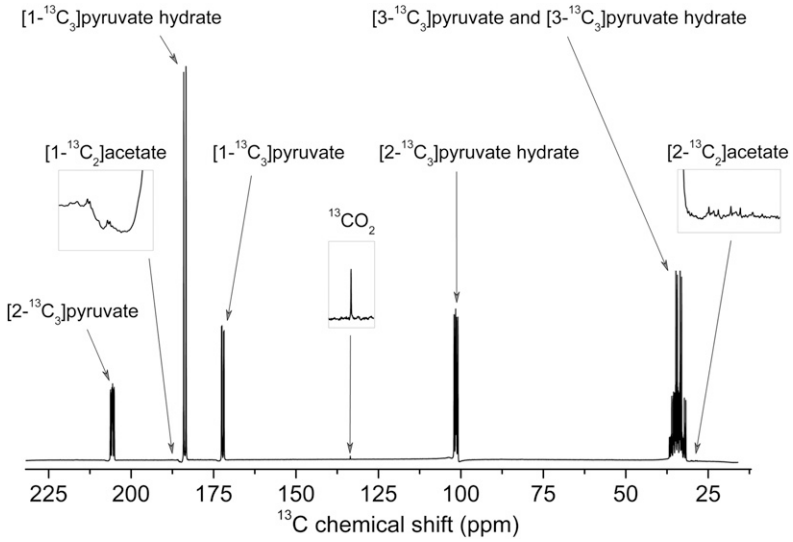

Fig. 2. ^{13}C MR spectrum of dissolved UV-irradiated [U-^{13}C]PA. Room-temperature high-resolution ^{13}C MR spectrum of UV-irradiated (60-min irradiation at 77 K) uniformly ^{13}C-labeled PA melted in D_2O (0.9 M) measured in a 400-MHz MR spectrometer.

of [1-^{13}C]pyruvate and its metabolic product [1-^{13}C]lactate (Fig. 4 *B* and *C*).

The fact that it is possible, in frozen pure PA, to accumulate by photoexcitation a radical concentration that is sufficiently large to enhance the ^{13}C nuclear polarization via dissolution DNP and obtain in vivo ^{13}C MR images with an SNR comparable to what can be obtained using persistent radicals is most likely related to the high efficiency of the radical creation and stabilization mechanisms. Following dissolution, only about one molecule of by-product is formed per radical stabilized at low temperature and all other PA molecules are intact (*Methods*). This would not likely be the case with standard photolabile radical precursors; our own attempt to obtain similar results with azo compounds was unsuccessful (even in frozen aqueous solutions containing up to 0.6 M azo compounds, most precursors were consumed after 1 h of photoexcitation and only 1–2 mM of radicals was detectable at low temperature).

Metabolic imaging based on hyperpolarized MR is establishing itself as a promising biomedical imaging technique and its clinical potential in oncology and cardiology has already been highlighted (17, 18, 26). We have demonstrated that there is no need to incorporate complex and potentially toxic chemicals into PA to hyperpolarize its ^{13}C spins because its intrinsic photochemical properties can be used to transform some of the PA molecules themselves into very efficient polarizing agents. The resulting dissolved hyperpolarized ^{13}C-labeled pyruvate solution is uncontaminated by paramagnetic impurities such as persistent radicals or any other nonendogenous substance and can thus be safely injected as MRI agent for in vivo metabolic imaging. Although there should be no fundamental difficulty in implementing the herein proposed method to produce sterile hyperpolarized pyruvate solutions, some technical developments will be required to adapt it for use in conjunction with an instrument such as the polarizer designed for clinical use (27). It would also most likely be cost efficient to replace the use of fairly costly persistent radicals by UV irradiation for in vitro NMR and preclinical MRI applications because up to 2 g of UV-irradiated PA can be prepared in only 1 h, whereas the typical lifetime of a UV light-emitting diode (LED) source is on the order of 20,000 h (*Methods*).

Methods

Radical Generation in Frozen PA. Droplets of 2 ± 0.5 μL pure natural abundance, [1-^{13}C] or [U-^{13}C] PA (Sigma-Aldrich) were poured one by one into a synthetic quartz dewar (Wilmad 150-mL Suprasil Dewar Flask type WG-850-B-Q) filled with liquid nitrogen to form frozen beads of about 1.5 mm diameter. The tail of the synthetic quartz dewar contained a 3-mm-inner-diameter quartz tube (Wilmad 705-PQ-6.25) into which a dozen beads were collected. The frozen beads were then irradiated 4 times for 15 min (the synthetic quartz dewar was rotated by 90° each 15 min to ensure that all beads were homogeneously irradiated) at 77 K using a high-power 365-nm LED array (Hamamatsu LC-L5). After completion of the irradiation, the beads were transferred into a glassware for storage in liquid nitrogen. No significant reduction in radical concentration was observed after 1 mo of storage at 77 K and the beads can thus be prepared weeks before the dissolution DNP experiments. The typical amount of UV-irradiated PA prepared during each 1-h irradiation was 0.4 g, but the setup allows for the preparation of up

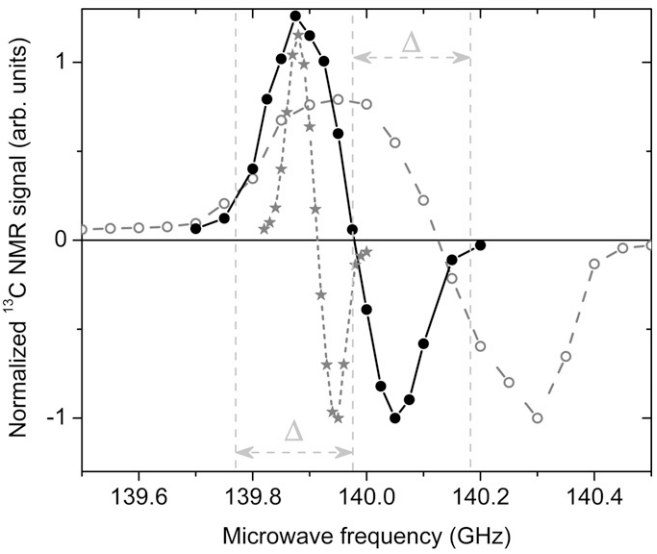

Fig. 3. Microwave spectra at 5 T and 4.2 K. Comparison between the microwave spectra measured by ^{13}C MR in UV-irradiated [1-^{13}C]PA (full circles), [1-^{13}C]PA doped with 16-mM OX063 trityl radicals (stars), and a frozen 3-M sodium [1-^{13}C]pyruvate aqueous solution doped with 50 mM TEMPO nitroxyl radicals (open circles). The frequency separation Δ between the central and the left or right vertical dotted lines corresponds to the ^{1}H MR frequency at 5 T.

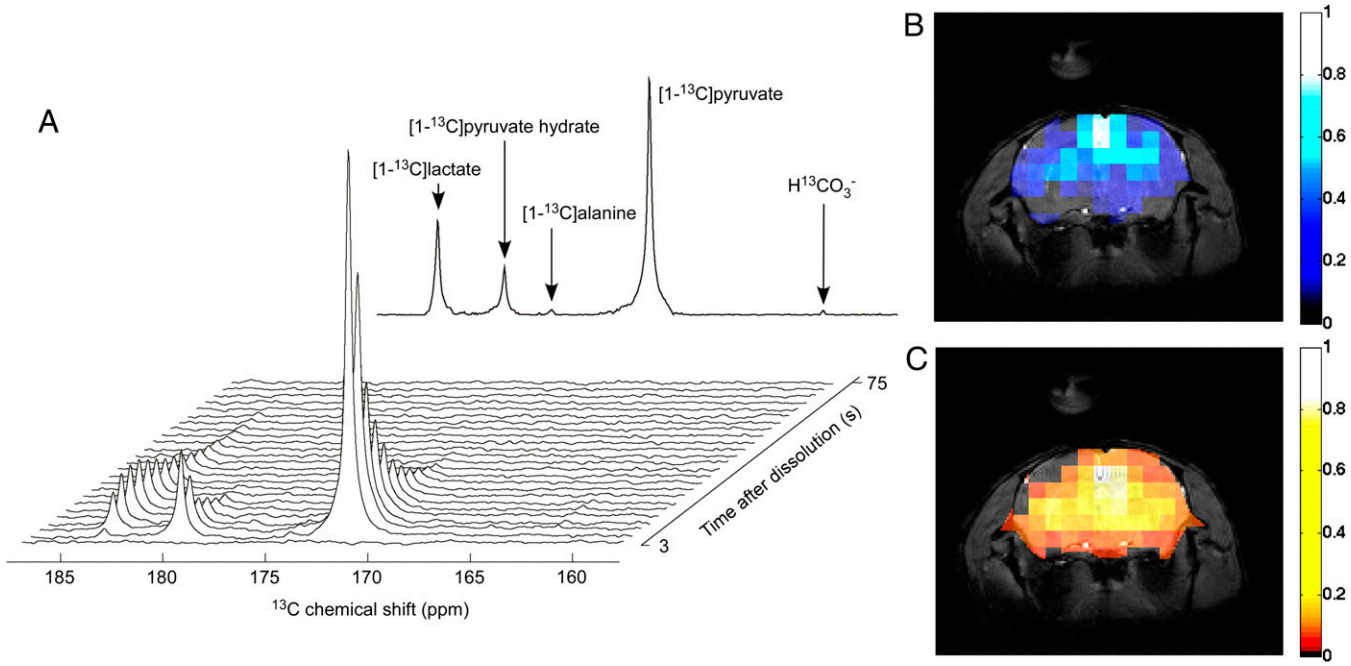

Fig. 4. In vivo real-time pyruvate metabolism. In vivo ^{13}C MR data recorded following the injection of 300 μL of 80 ± 5 mM [1-^{13}C]pyruvate solution hyperpolarized by DNP using polarizing agents created by UV irradiation. (*A*, *Upper*) Series of ^{13}C spectra acquired in the mouse head every 3 s. (*A*, *Lower*) Sum of all 25 displayed spectra. (*B* and *C*) The 5-mm^3 resolution bSSFP ^{13}C images recorded using interleaved selective excitations of [1-^{13}C]pyruvate (*B*) and [1-^{13}C]lactate (*C*) superimposed to ^{1}H anatomical images of the mouse head.

to 2 g/h and similar LED arrays with larger illumination area are commercially available if larger quantities are required.

X-Band ESR Measurements at 77 K. A weighted amount of several μL of frozen UV-irradiated pure natural abundance or [1-^{13}C] PA was placed inside a 4-mm-inner-diameter quartz tube (Wilmad 707-SQ-100M) plunged inside a synthetic quartz dewar (Wilmad 150-mL Suprasil Dewar Flask type WG-850-B-Q) filled with liquid nitrogen. The tail of the synthetic quartz dewar was placed inside the resonator of an X-band ESR spectrometer (Bruker EMX). The ESR signal integral of a set of frozen aqueous samples containing known concentrations (between 1 and 10 mM) of TEMPO (2,2,6,6-Tetramethylpiperidoxyl) nitroxyl radical was measured as reference to determine the radical concentration of the UV-irradiated PA samples. ESR measurements of the UV-irradiated PA samples were performed after each of the six 1- min irradiation time intervals and the radical concentration was plotted as a function of the total irradiation time (Fig. 1*A*).

High-Resolution ^{13}C MR Measurements of Melted UV-Irradiated [U-^{13}C]PA. To determine the exact chemical composition of the solutions obtained after dissolving the beads, high-resolution ^{13}C MR measurements were performed. Seven frozen beads of UV-irradiated [U-^{13}C]PA (total weight of 35.9 mg) containing 17.5 ± 0.3 mM of radicals (concentration determined via ESR measurements) were melted in a glassware filled with 448.0 mg D_2O to obtain a 900-mM solution that was placed inside a 5-mm glass tube (Wilmad, 527-PP-9). The pH of the solution was measured to be 1. The room-temperature (25 °C) ^{13}C spectrum of the solution was recorded on a DRX-400 spectrometer (Bruker BioSpin SA) using a broadband observe (BBO) 5-mm probe with a single radiofrequency (rf) pulse sequence using the following parameters: pulse length of 15 μs at power of −5 dB, repetition delay of 180 s, and total number of scans of 512.

The J couplings determined from the ^{13}C spectrum were $^{1}J(^{13}C,^{1}H)$ = 130 Hz, $^{1}J(^{13}C,^{13}C)$ = 43 Hz, and $^{2}J(^{13}C,^{13}C)$ = 3 Hz for the methyl ^{13}C of [U-^{13}C] pyruvate and $^{1}J'(^{13}C,^{1}H)$ = 130 Hz and $^{1}J'(^{13}C,^{13}C)$ = 44 Hz for the methyl ^{13}C of [U-^{13}C]pyruvate hydrate (Fig. S3), which are consistent with published values for [U-^{13}C]pyruvate (13, 28, 29). The J couplings deduced from the small peaks observed in the methyl region of the ^{13}C spectrum [$^{1}J(^{13}C,^{1}H)$ = 125 Hz and $^{1}J(^{13}C,^{13}C)$ = 55 Hz] correspond to the values reported for the methyl ^{13}C of [1,2-$^{13}C_2$]acetic acid (Fig. S4) (28–30). The chemical shift of the narrow peak observed at 126 ppm was assigned to the ^{13}C resonance of $^{13}CO_2$ (31).

By comparing the integrals of the [1,2-$^{13}C_2$]acetic acid and $^{13}CO_2$ signals to the signal integral of [U-^{13}C]pyruvate (including its hydrate form), it was deduced that the concentration of [1,2-$^{13}C_2$]acetic acid and $^{13}CO_2$ was 1.5 ± 0.05 and 1.45 ± 0.05 mM, respectively, values that are 600× smaller than the [U-^{13}C]pyruvate concentration. The pyruvate to by-products concentration ratio in the melted samples (900/1.5 = 600) is thus almost equal to the PA to radical concentration ratio in the frozen pure PA UV-irradiated samples (13,500/17.5 = 770). This demonstrates that nearly all radicals created in the frozen state are stable at 77 K and only recombine when the sample is melted.

Solid-State DNP Measurements at 5 T and 1.2 K. Five beads were placed inside the 0.4-mL polytetrafluoroethylene (PTFE) sample cup of the 5-T in-house–designed polarizer described in previous publications (23, 25). The sample cup was inserted inside the polarizer filled with about 0.5 L liquid helium at atmospheric pressure (4.2 K). The microwave power at the output of the source was set to 50 mW for all experiments. The ^{13}C nuclear polarization was monitored by means of pulsed NMR using 2° tipping pulses. The microwave spectrum was measured at 4.2 K and compared with the microwave spectra of [1-^{13}C]PA doped with 16 mM Ox063 trityl radicals and a 4.5-M sample of sodium [1-^{13}C]pyruvate (1:2 ethanol-d_6:D_2O) doped with 50 mM TEMPO radicals (Fig. 3). The irradiation frequency was set to 139.85 GHz, a value leading to the largest ^{13}C polarization enhancement, and the vacuum pumps were turned on to lower the temperature of the sample space to maintain the frozen sample under superfluid helium at 1.2 ± 0.05 K. The measured build-up time at 1.2 K was 1,920 ± 120 s and the solid-state polarization after 2.5 h was 10 ± 1%.

Dissolution and Transfer of DNP-Enhanced PA. The DNP-enhanced frozen PA beads (~30 μL) were dissolved in 6 mL of superheated (170 °C) buffer solution containing 80 mM NaOH and 40 mM Tris (2-Amino-2-hydroxymethyl-propane-1,3-diol) by means of the dissolution method described by Ardenkjaer-Larsen et al. (3). In the system used for the present study, pressurized helium gas drives the resulting solution out of the polarizer through a 6-m-long capillary into the bore of a 31-cm horizontal-bore actively shielded 9.4-T magnet (Magnex Scientific), where the sample is collected in a remotely controlled in-house–designed separator/infusion pump that separates the liquid solution from the gas (23, 32). The transfer time was set to 2 s with a helium gas pressure of 6 bar (33). A volume of 0.6 mL PBS solution was inserted inside the separator/infusion pump before dissolution.

The pH value of the resulting hyperpolarized pyruvate solutions was measured to be 7.2 ± 0.2. At the end of each dissolution experiment (including in vivo experiments), 200 μL of the residual solution was collected from the infusion pump and the [1-^{13}C]pyruvate concentration was measured in a high-resolution DRX-400 spectrometer (Bruker BioSpin SA) by comparing the signal with a reference sample of known concentration.

In Vitro Hyperpolarized ^{13}C MRS Measurements. In vitro hyperpolarized ^{13}C MRS measurements were carried out inside an in-house–designed separator/infusion pump using NMR coils (^{1}H and ^{13}C) implemented on the pump (33). The static magnetic field inside the separator/infusion pump was shimmed before the dissolution DNP experiments over a reference PA solution using the ^{1}H coil and the fast automatic shimming technique by mapping along projections (FASTESTMAP) protocol (34). The pH of the solution inside the separator/infusion pump was 7.1 (0.6 mL of PBS solution was inserted inside the separator/infusion pump before dissolution). A series of 5° pulses separated by a 3-s delay was applied to measure the signal decay as a function of time (Fig. S1). The delay between dissolution and NMR measurements was set to 3 s. All measurements were performed in the 31-cm horizontal-bore actively shielded 9.4-T magnet on a Direct Drive spectrometer (Agilent). The observed characteristic signal decay corresponded to a ^{13}C T_1 of 53 ± 2 s. This value is in agreement with published in vitro T_1 values measured at 9.4 T in D_2O at pH 7 (13).

Animal Preparation. In vivo experiments were performed on male Naval Medical Research Institute (NMRI) mice (54.5 ± 6 g). All animal experiments were conducted according to federal and local ethical guidelines, and the protocols were approved by the local regulatory body of the Canton Vaud, Switzerland (Service de la consommation et des affaires vétérinaires, Affaires vétérinaires, Canton de Vaud, Suisse). Animals were anesthetized with 1.5% isoflurane in oxygen. A femoral vein was catheterized for injection of hyperpolarized [1-^{13}C]pyruvate. The mouse was placed on a holder along with the infusion/separator pump and the femoral vein catheter was connected to the outlet of the pump. The holder was subsequently inserted inside the scanner. The pump was programmed to automatically inject a bolus of 300 μL of solution containing 80 ± 5 mM of hyperpolarized [1-^{13}C]pyruvate within 5 s. Mouse physiology was monitored during the entire experiment: body temperature was stabilized between 37 and 38 °C while respiration rate was maintained at 100 min^{-1} by adjustment of the isoflurane dose. The rate and dose of the injection was determined in bench experiments to ensure that the bolus-like injection does not affect mouse physiology. After the experiment, animals were euthanized with a lethal dose of pentobarbital.

In Vivo Hyperpolarized ^{13}C MRS and Imaging Measurements. All measurements were performed on the Direct Drive spectrometer interfaced to the 31-cm horizontal-bore actively shielded 9.4-T magnet. rf transmission and reception was done using an in-house–designed hybrid probe consisting of a pair of 10-mm-diameter ^{1}H surface coils in quadrature and an 8-mm-diameter ^{13}C surface coil. These coils were placed on top of the mouse head. The ^{13}C spectra were acquired through single-pulse experiments with adiabatic rf pulses (35). To generate an external ^{13}C reference signal, a small sphere filled with 99% ^{13}C-labeled formic acid was placed in the center of the ^{13}C coil. The acquisition time was set to 200 ms. High-order shimming was performed using the FASTESTMAP algorithm (34). Following the dissolution, transfer, pH adjustment, and injection of 300 μL of hyperpolarized [1-^{13}C]pyruvate in 5 s, the acquisition was triggered by the polarizer electronics. The ^{13}C signals of [1-^{13}C]pyruvate and [1-^{13}C]lactate decayed with a time constant of 19 ± 3 s and 41.5 ± 4 s, respectively (Fig. 4*A*). These values are comparable to the ones observed in previous studies performed in rats (11, 13).

The ^{13}C images were acquired using a 3D frequency-selective bSSFP sequence with a repetition time (TR) equal to 2× the echo time (TE). An [α /2 – TR/2] preparation module consisting of an α /2-pulse followed by a TR/2 delay was used to prevent large signal variations while approaching the steady state. This preparation module was immediately followed by an alternating ± α-pulse train. Each excitation pulse was separated from the next one by TR as previously described (36). A flip-back [TR/2 – α/ 2] module that is identical to the time-reversed [α/2 – TR/2] module was used to store the remaining steady-state magnetization in the longitudinal direction at the end of the bSSFP pulse train. Imaging parameters were the following: matrix = 32 × 32, field of view = 30 × 30 mm^2, slice = 5 mm, TR/TE = 5.6/2.8 ms. Imaging was performed with Gaussian-shaped rf pulses (duration 2 ms). Images were alternatively acquired at the frequency of [1-^{13}C]pyruvate using a 10° flip angle and at the frequency of [1-^{13}C]lactate using a 30° flip angle. Each acquisition is separated by 1.5 s, meaning a time resolution for each metabolite of 3 s for a total acquisition time of 45 s.

Before 2D fast Fourier transform reconstruction, the data were apodized with a Hamming window. Anatomical proton MR images were acquired using a 3D gradient echo sequence. Imaging parameters were the following: matrix = 256 × 256, field of view = 30 × 30 mm^2, slice = 0.5 mm, TR/TE = 25/5.4 ms, flip angle = 30°. The ^{13}C metabolic images superimposed to the proton anatomical images (Fig. 4 *B* and *C*) were obtained by summing three and four consecutive [1-^{13}C]pyruvate and [1-^{13}C]lactate images, respectively. All data were processed using MATLAB.

ACKNOWLEDGMENTS. The authors thank Dr. J. J. van der Klink and Prof. R. Gruetter for initiating the DNP projects in Lausanne and for their support, and the Sample Environment and Polarised Targets group of the Paul Scherrer Institute for providing the polarizer cryostat and for granting access to the X-band ESR spectrometer. They also thank M. H. Lerche for providing the PA sample doped with OX063 trityl radicals for the microwave spectrum measurements. This work was supported by the Swiss National Science Foundation (Grants PP00P2_133562 and 200020_144424), the National Competence Center in Biomedical Imaging, the Centre d'Imagerie BioMédicale of the Université de Lausanne, Université de Genève, Hôpitaux Universitaires de Genève, Centre Hospitalier Universtaire Vaudois, Ecole Polytechnique Fédérale de Lausanne, and the Leenards and Jeantet Foundations.

1. Shulman RG, Rothman DL (2001) 13C NMR of intermediary metabolism: Implications for systemic physiology. *Annu Rev Physiol* 63:15–48.
2. Abragam A, Goldman M (1978) Principles of dynamic nuclear-polarization. *Rep Prog Phys* 41(3):395–467.
3. Ardenkjaer-Larsen JH, et al. (2003) Increase in signal-to-noise ratio of > 10,000 times in liquid-state NMR. *Proc Natl Acad Sci USA* 100(18):10158–10163.
4. Gallagher FA, Kettunen MI, Brindle KM (2009) Biomedical applications of hyperpolarized C-13 magnetic resonance imaging. *Prog Nucl Magn Reson Spectrosc* 55(4):285–295.
5. Gallagher FA, et al. (2009) Production of hyperpolarized [1,4-13C2]malate from [1,4-13C2]fumarate is a marker of cell necrosis and treatment response in tumors. *Proc Natl Acad Sci USA* 106(47):19801–19806.
6. Golman K in't Zandt R, Thaning M (2006) Real-time metabolic imaging. *Proc Natl Acad Sci USA* 103(30):11270–11275.
7. Mishkovsky M, Comment A, Gruetter R (2012) In vivo detection of brain Krebs cycle intermediate by hyperpolarized magnetic resonance. *J Cereb Blood Flow Metab* 32(12):2108–2113.
8. Schroeder MA, et al. (2009) Real time, in vivo observation of oxidative carbohydrate metabolism reveals the key regulatory role of acetyl-carnitine as a substrate buffer in the heart. *Circulation* 120(18):S855–S856.
9. Albers MJ, et al. (2008) Hyperpolarized 13C lactate, pyruvate, and alanine: Noninvasive biomarkers for prostate cancer detection and grading. *Cancer Res* 68(20):8607–8615.
10. Day SE, et al. (2007) Detecting tumor response to treatment using hyperpolarized 13C magnetic resonance imaging and spectroscopy. *Nat Med* 13(11):1382–1387.
11. Hurd RE, et al. (2010) Cerebral dynamics and metabolism of hyperpolarized [1-(13)C] pyruvate using time-resolved MR spectroscopic imaging. *J Cereb Blood Flow Metab* 30(10):1734–1741.
12. Lau AZ, et al. (2013) Noninvasive identification and assessment of functional brown adipose tissue in rodents using hyperpolarized (13)C imaging. *Int J Obes (Lond)*, 10.1038/ijo.2013.58.
13. Marjańska M, et al. (2010) In vivo 13C spectroscopy in the rat brain using hyperpolarized [1-(13)C]pyruvate and [2-(13)C]pyruvate. *J Magn Reson* 206(2):210–218.
14. Park I, et al. (2010) Hyperpolarized 13C magnetic resonance metabolic imaging: Application to brain tumors. *Neuro Oncol* 12(2):133–144.
15. Park JM, et al. (2013) Metabolic response of glioma to dichloroacetate measured in vivo by hyperpolarized (13)C magnetic resonance spectroscopic imaging. *Neuro Oncol* 15(4):433–441.
16. Schroeder MA, et al. (2013) Hyperpolarized (13)C magnetic resonance reveals early- and late-onset changes to in vivo pyruvate metabolism in the failing heart. *Eur J Heart Fail* 15(2):130–140.
17. Kurhanewicz J, et al. (2011) Analysis of cancer metabolism by imaging hyperpolarized nuclei: Prospects for translation to clinical research. *Neoplasia* 13(2):81–97.
18. Nelson SJ, et al. (2013) Metabolic imaging of patients with prostate cancer using hyperpolarized [1-13c]pyruvate. *Sci Transl Med* 5(198):198ra108.
19. Budac D, Wan P (1992) Photodecarboxylation - mechanism and synthetic utility. *J Photochem Photobiol A* 67(2):135–166.
20. Leermakers PA, Vesley GF (1963) Photolysis of pyruvic acid in solution. *J Org Chem* 28(4):1160–1161.
21. Lieben F, Lowe L, Bauminger B (1934) The decomposition of high polymer carbohydrate as well as lactic acid and pyruvic acid in the light of quartz lamps. *Biochem Z* 271:209–212.

22. Skutches CL, Holroyde CP, Myers RN, Paul P, Reichard GA (1979) Plasma acetate turnover and oxidation. *J Clin Invest* 64(3):708–713.
23. Comment A, et al. (2007) Design and performance of a DNP prepolarizer coupled to a rodent MRI scanner. *Concepts Magn Reson* 31B(4):255–269.
24. Jóhannesson H, Macholl S, Ardenkjaer-Larsen JH (2009) Dynamic nuclear polarization of [1-13C]pyruvic acid at 4.6 tesla. *J Magn Reson* 197(2):167–175.
25. Jannin S, et al. (2008) A 140 GHz prepolarizer for dissolution dynamic nuclear polarization. *J Chem Phys* 128(24):241102.
26. Malloy CR, Merritt ME, Sherry AD (2011) Could 13C MRI assist clinical decision-making for patients with heart disease? *NMR Biomed* 24(8):973–979.
27. Ardenkjaer-Larsen JH, et al. (2011) Dynamic nuclear polarization polarizer for sterile use intent. *NMR Biomed* 24(8):927–932.
28. Frei K, Bernstein HJ (1963) Carbon-carbon spin-coupling constants in characteristic CC-bond types. *J Chem Phys* 38(5):1216–1226.
29. Karabatsos G (1961) Spin-spin coupling constants between non-bonded C13 and protons in some C13-labeled compounds. *J Am Chem Soc* 83(5):1230–1232.
30. Mishkovsky M, Cheng T, Comment A, Gruetter R (2012) Localized in vivo hyperpolarization transfer sequences. *Magn Reson Med* 68(2):349–352.
31. Fulmer GR, et al. (2010) NMR chemical shifts of trace impurities: Common laboratory solvents, organics, and gases in deuterated solvents relevant to the organometallic chemist. *Organometallics* 29(9):2176–2179.
32. Comment A, van der Klink J (2011) US Patent 8,034,027.
33. Cheng T, et al. (2013) Automated transfer and injection of hyperpolarized molecules with polarization measurement prior to in vivo NMR. *NMR Biomed*, 10.1002/nbm.2993.
34. Gruetter R, Tkác I (2000) Field mapping without reference scan using asymmetric echo-planar techniques. *Magn Reson Med* 43(2):319–323.
35. Staewen RS, et al. (1990) 3-D FLASH imaging using a single surface coil and a new adiabatic pulse, BIR-4. *Invest Radiol* 25(5):559–567.
36. Scheffler K, Lehnhardt S (2003) Principles and applications of balanced SSFP techniques. *Eur Radiol* 13(11):2409–2418.